Comparison of island and axisymmetric divertor

Ralf Schneider†, Hermann Renner†, David Coster‡ and Josef Neuhauser‡§

† Max-Planck-Institut für Plasmaphysik, EURATOM Association, Wendelsteinstr.1, D-17491 Greifswald, Germany

‡ Max-Planck-Institut für Plasmaphysik, EURATOM Association, D-85748 Garching, Germany

Abstract. The need for sufficient power and particle exhaust is common for all magnetic confinement concepts. For the new stellarator W7-X an island divertor is planned making use of the intrinsic island structure at the edge.

The concept of the W7-X island divertor (as a prototype of general island divertors) and its specific design criteria will be discussed. A comparison with axisymmetric divertors (specifically with the ASDEX-Upgrade Div-II configuration) of the basic physics guidelines for divertor design will be made. The common elements (general scrape-off layer physics due to the dominant parallel transport and atomic physics effects through neutrals) and possible differences (3D effects, differences in fieldline geometries, additional flexibility through divertor coils, possible ergodicity in some configurations, core baffling of neutrals) will be discussed.

Submitted to: *Plasma Phys. Control. Fusion*

§ Correspondance to: Ralf.Schneider@ipp.mpg.de

1. Introduction

The need for sufficient power and particle exhaust is common for all magnetic confinement concepts. The stellarator W7-X [1] presently under construction at Greifswald, Germany, is a large advanced stellarator of the HELIAS-type with strongly varying plasma cross-section ($R = 5.5\,m, a = 0.55\,m, B_0 = 3\,T$, 5 periods, moderate shear and variable rotational transform $5/6 \leq \iota \leq 5/4$ at the boundary). The advanced stellarator concept [1] eliminates the shortcomings of the classical stellarator approach like W7-A [2]. The generation of these 3D magnetic configurations for W7-X will be obtained by modular twisted superconducting coils allowing quasi steady-state operation. The basic heating system will be a $140\,GHz$ ECR cw heat source of $10\,MW$. Additional heating schemes, ICRF and NBI, will be provided for flexible experimentation.

2. Edge exhaust principles

The basic idea of any edge exhaust concept is to utilize the fact that the dominant parallel heat conduction by electrons along magnetic fieldlines directs the power flow onto dedicated surfaces (target plates). There, the plasma interacts with the walls releasing neutrals into the plasma which then get ionized by the plasma. By keeping these neutrals trapped in specific regions (either by using geometrical limitations by baffles together with the plasma or relying completely on plasma plugging alone) a recycling cycle is triggered self-enhancing the plasma particle flow onto the target plates through the ionization plasma source of the neutrals. By this, plasma density increases and plasma temperature drops reducing by this the release of impurities into the plasma due to the reduction of physical sputtering. For a reduction of the power flux density on the target plates to technically tolerable values (below about $10\,MW/m^2$) radiation losses (both from hydrogen or intrinsic impurities) are used, rising with plasma density.

For the existence of good confinement the favourable configurations are those where the X-point is away from the bad curvature region [3].

The major technical limit for any divertor is the limitation of the target plate power load $q_{\perp,targetplate}$ due to the very small radial energy decay length to technically controllable values (below about $10\,MW/m^2$)

$$q_{\perp,targetplate} = \frac{P_\alpha}{2\pi R_{X-point} \cdot N_{Div} \Delta_e},$$

where Δ_e is the energy decay length at the target plate, P_α is the heating power entering the scrape-off layer (for ITER the α-power), N_{Div} the number of active divertors and $R_{X-point}$ the (average) X-point radius.
For nominal ITER operation numbers one gets about $150\,MW/m^2$ [3]. Further reduction factors are bulk radiation (0.8) and poloidal tilting of target plates (0.5-0.25), but the resulting $q_{\perp,targetplate} = 35\,MW/m^2$ is still well above realistic values for steady-state operation which are below about $10\,MW/m^2$. Therefore additional losses are required

to spread the power over a larger area. Neutral recycling losses are not large enough [4], mainly because the interaction with neutrals is mainly a surface effect. CX losses are only effective at high temperatures (100% at 660 eV, 6% at 100 eV, 0.2% at 10 eV). Additionally, CX neutrals from the hot regions (divertor throat, main plasma) pose erosion problems. For neutral hydrogen radiation above about 8 eV, the ratio of energy radiated to that required to ionize the atom is around 2-3. For low temperatures, to maintain a high heat flux, temperature gradients are steep ($q_{\|} \sim T^{5/2}\nabla T$). Therefore, the low temperature region is very small. Finally, volume recombination is only important below about 2 eV. As a consequence, additional impurity losses are necessary. Two point models for variation along field lines [4, 5, 6, 7] demonstrate the connection between radiation losses and momentum drop and show that momentum loss from plasma increases the radiation loss capability. Using either experimental results, simple estimates or modelling results one sees that momentum removal is effective only below about 5 eV [8]. Here, ionisation gets unimportant, neutrals can freely interpenetrate the plasma flow. CX momentum loss is still confined to a boundary layer with thickness $\lambda_{CX,0}$ and for deeper layers CX enhances perpendicular viscosity and ion-energy cross-diffusion.

The different divertor operation regimes can be summarised as follws: starting from low recycling conditions (divertor transparent for neutrals, high temperatures at the target plates, practically no parallel gradient) one moves to high-recycling (attached) conditions (opaque divertor, temperature reduction due to recycling losses, enhanced density at the plate, no energy detachment, neutral mean free path $\lambda_0 \ll$ SOL width, radial gradients $\approx$ SOL width $\ll$ parallel gradients, radial flows $\ll$ parallel flows). The next regime (below about 5 eV) is then layer detachment, which is practically identical to the high-recycling regime, however momentum losses from CX with neutrals are already slowing down the plasma flow and energy losses get quite important. The final regime is then the flame detachment (complete detachment) below about 2 eV where the onset of volume recombination creates a virtual target inside the plasma where all the plasma fluxes are stopped by the recombination (this process is rather slow and works only if the flow is already slow enough due to CX friction with neutrals). It is characterised by a complex 2-D situation: $\lambda_0 \geq$ SOL width, radial gradients $\approx$ SOL width $\approx$ parallel gradients, radial flows $\approx$ parallel flows, energy detachment, complete momentum detachment, large reduction of particle flow to the plate, shift of density maximum away from the plate into the plasma.

In the following we will estimate the divertor temperature necessary for safe operation (about $5\,MW/m^2$). Starting with an equation for the residual charged particle energy flux to the target plate,

$$q_{\|,targetplate} = M_d n_{e,d} \sqrt{\frac{(\gamma+1)kT_{e,d}}{\mu m_{prot}}} (\delta_{eff} kT_{e,d} + \epsilon_{ion})$$

$$q_{\|,targetplate} \sim p_{e,d} \sqrt{T_{e,d}} (\delta_{eff} k + \frac{\epsilon_{ion}}{T_{e,d}}),$$

where M_d, $n_{e,d}$ and $T_{e,d}$ are Mach number, electron density and temperature at the plate, γ is the adiabatic constant, μm_{prot} is the ion mass, δ_{eff} is the electron energy transfer coefficient and ϵ_{ion} is the effective ionization energy (including radiation losses from hydrogen as an enhancement). Using momentum balance (if there is no momentum loss out of the fan and the assumption $T_i = T_e$),

$$p_b = 2p_{e,d} + p_0,$$

the mid-plane pressure p_b is balanced by the sum of twice the divertor electron pressure and the neutral pressure at the plate. Particle balance determines the ratio of plasma to neutral pressure, (particle flow to the target = total ionization in a plasma column perpendicular to the plate)

$$M_d n_{e,d} \sqrt{\frac{(\gamma+1)kT_{e,d}}{\mu m_{prot}}} sin\alpha = \int_0^\infty n_e \langle \sigma_{ion} v_{th,e} \rangle n_0 dx.$$

Using a simple neutral diffusion model in the perpendicular direction away from the plate (CX gives rise to diffusion and ionisation to the loss of neutrals)

$$\frac{d}{dx} \lambda_{CX} v_{th,0} \frac{dn_0}{dx} = n_e \langle \sigma_{ion} v_{th,e} \rangle n_0$$

reproduces the well known result for the spatial distribution of neutrals

$$n_0(x) = n_{0,d} e^{-\xi / \sqrt{\lambda_{ion,0} * \lambda_{CX,o}}}$$

in terms of CX and ionisation mean-free paths at reference electron density $n_e d$ in the coordinate

$$\xi = \int_0^x n_e / n_{e,d} dx.$$

The total ionisation rate (per unit area and for an optically thick SOL) becomes

$$\int_0^\infty n_e \langle \sigma_{ion} v_{th,e} \rangle n_0 dx = n_{0,d} v_{th,0} \sqrt{\frac{\lambda_{CX,0}}{\lambda_{ion,0}}}$$

or

$$\int_0^\infty n_e \langle \sigma_{ion} v_{th,e} \rangle n_0 dx = \frac{p_0}{\sqrt{T_0}} \sqrt{\frac{\gamma k}{\mu m_{prot}}} \sqrt{\frac{\lambda_{CX,0}}{\lambda_{ion,0}}}.$$

This gives a relation between neutral and plasma pressure, resulting in

$$q_{\parallel, targetplate} = 10^4 \sqrt{\frac{\gamma}{\mu}} p_\mathrm{b} \frac{\Theta M}{2\Theta \sqrt{\frac{\gamma}{\gamma+1}} + M \sin\alpha} \sqrt{T_{e,d}} (\delta_{eff} + \frac{\epsilon_{ion}}{T_{e,d}})$$

where

$$\Theta = \sqrt{\frac{T_{e,d}}{T_0}} \sqrt{\frac{\lambda_{\mathrm{CX}_0}}{\lambda_{\mathrm{ion}_0}}}$$

For typical ITER conditions ($n_{e,b} = 0.5 - 1.0 \cdot 10^{20}\, m^{-3}, T_e = 100 - 500eV$) the operational point for a desired heat flux value of $5MW/m^2$ lies in a temperature range between 1 and 3 eV. In this temperature range the onset of volume recombination and the creation of a virtual target by this process inside the plasma in front of the real target is important. Operation in at least semi-detached operation is required. Analysis of this detached regime shows that conservation laws along fieldlines determine a scrape-off layer based fuelling limit [9] of the upstream (midplane) density. Operation close to such an operational limit requires usually feedback control for avoidance of instabilities.

3. Optimization of the tokamak divertor

As a typical example the strategy for the optimization of the tokamak divertor, ASDEX-Upgrade is shortly summarized here.

The original open divertor structure was changed to a closed geometry. The basic idea for the design of the new divertor was to maximize the neutral losses in the region close to the separatrix (where most of the heat flux is conducted into the divertor) by reflection of neutrals towards the separatrix using strongly inclined target plates [10].

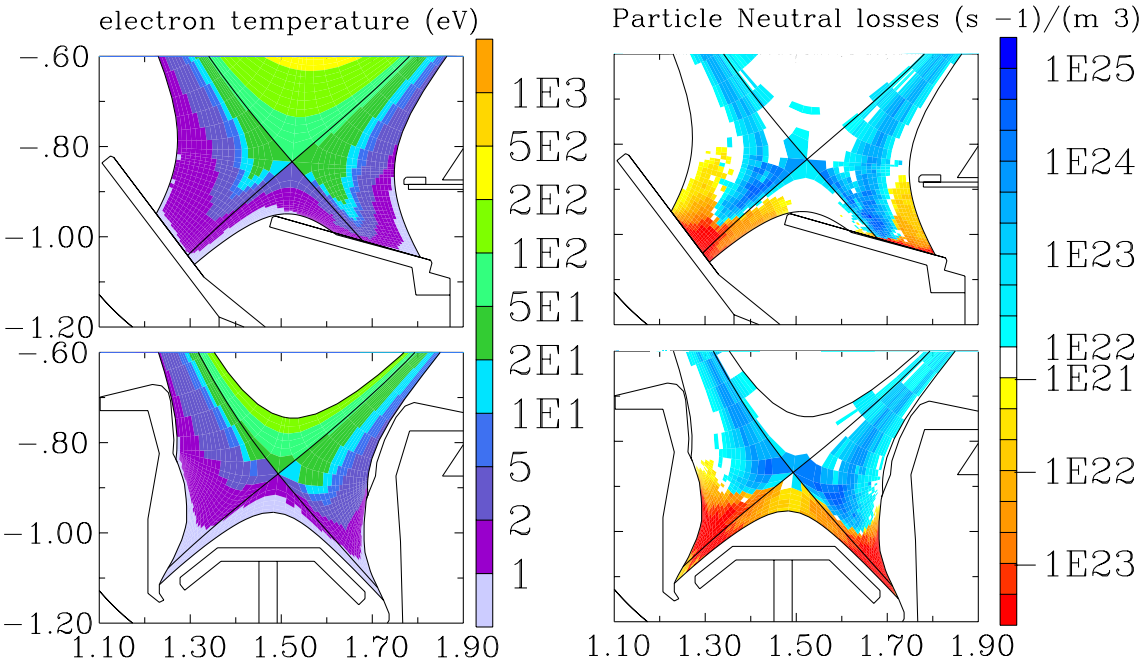

Figure 1. Contour plots of electron temperature (left column) and neutral particle source (right column) for ASDEX Upgrade DivI (top) and DivII (bottom) from B2-Eirene simulations for same upstream conditions. The ionization sources for the plasma are shown in blue, the recombination losses in red. Target plates and baffles as well as magnetic separatrix are shown.

Comparing the contour plots of electron temperature and neutral particle sources by ionization and recombination for same upstream conditions (Fig. 1) one gets lower temperatures and a larger amount of volume recombination for Div-II, especially in the high power flux region close to the separatrix. The strongly inclined target plates for DivII reflect neutrals preferentially towards this hot region and increase by this the neutral losses at the separatrix.

Additional baffle plates towards the main chamber are used to shield the core from divertor neutrals. The stability of this setup is guaranteed by the fact that detachment starts close to the separatrix at relatively low midplane densities (by this minimizing also the peak target loads) but staying attached up to the density limit in the far outer scrape-off layer, because all the neutrals created there getting reflected towards the separatrix and by this not driving the detachment of this outer part. An additional dome baffle in the private flux region is used for an improved particle exhaust capability by the pumps (minimizing the visible plasma surface for neutrals behind the dome and by this minimizing their ionization probability by the plasma which is the competing pump). This optimization process improved

the power exhaust capability by a factor of 2-4 [11, 12] and confirmed the predictive code design calculations with B2-Eirene. However, closed divertor operation naturally limits the experimental flexibility (not all MHD equilibria fit into the divertor slots) and diagnostic access (especially in the divertor region).

In contrast to the well understood divertor physics, the main chamber edge physics is much less clear. The physics is strongly determined by anomalous transport which itself is not yet theoretically (and quantatively) understood. For example, there is strong evidence, that the dominant source for main chamber neutral fluxes and core impurity concentration is an internal main chamber recycling cycle decoupled from divertor leakage [10]. Here, the creation of shoulder-like structures with strongly enhanced anomalous transport are of special interest for this effect. The existence of this internal main chamber recycling relaxes then strongly the requirement for divertor baffling to the main chamber, because one does not have to baffle the divertor much better (maybe a factor of 2 to 5) than this remaining neutral flux. Also, additional efforts have to concentrate on the minimisation of impurity fluxes from this source to improve the core purity.

In addition, the effect of ELMs has to be taken into account producing time-dependent power and particle flows onto the divertor, the baffles and the main chamber wall, which has to be taken care of.

4. W7-X edge exhaust concept

The W7-X concept for the edge exhaust makes use of the formation of an inherent separatrix at the boundary creating a so-called island divertor. The confinement region is either limited by the separatrix of islands (being intersected by target plates) or by an ergodised boundary with remnants of islands.

The X-lines in island divertors are helical, with the pitch depending on the resonant rotational transform of the island chain. The standard magnetic configuration of W7-X ($\iota = 1 = 5/5$ at the boundary) has five toroidally closed helical X-lines. For extended islands, the positioning of divertor elements along the helical edge (areas with strongest poloidal curvature of the magnetic surfaces) allows to concentrate the plasma flow on target plates and to separate the plasma-wall interaction from the plasma core.

For the start of W7-X an open divertor system [13] has been chosen to achieve effective power and particle exhaust in a wide magnetic configuration space and plasma parameter range (see Figs. 2). The deposition pattern as calculated by field-line tracing (accounting for the perpendicular transport with a field line diffusion term) depends on the twist and symmetry of the x-lines, but stays in all studied cases (variaton of ι and β) on the target areas. Additional baffle elements are foreseen to optimize the pumping capabilities of the cryopumps by maximizing the neutral densities in the divertor.

Additional divertor control coils are available to control the variation of the connection length and modify the distance between target plates and separatrix by changing the island size. Further application of these coils is the compensation of symmetry-breaking error-fields, e.g. due to small construction/installation inaccuracies. They also can be used to sweep the strike points on the target (10 kA currents are needed for a poloidal shift of the strike points on the target of about 5 cm). For specific configurations they can be used to enhance or reduce ergodic effects at the boundary.

An analysis of the properties of the stochastic layers in W7-X [14] showed that mean Kolomogorov length (the length on which two neighboring fieldlines diverges from each other exponentially) decreases with increasing β and by this ergodic effects get more important.

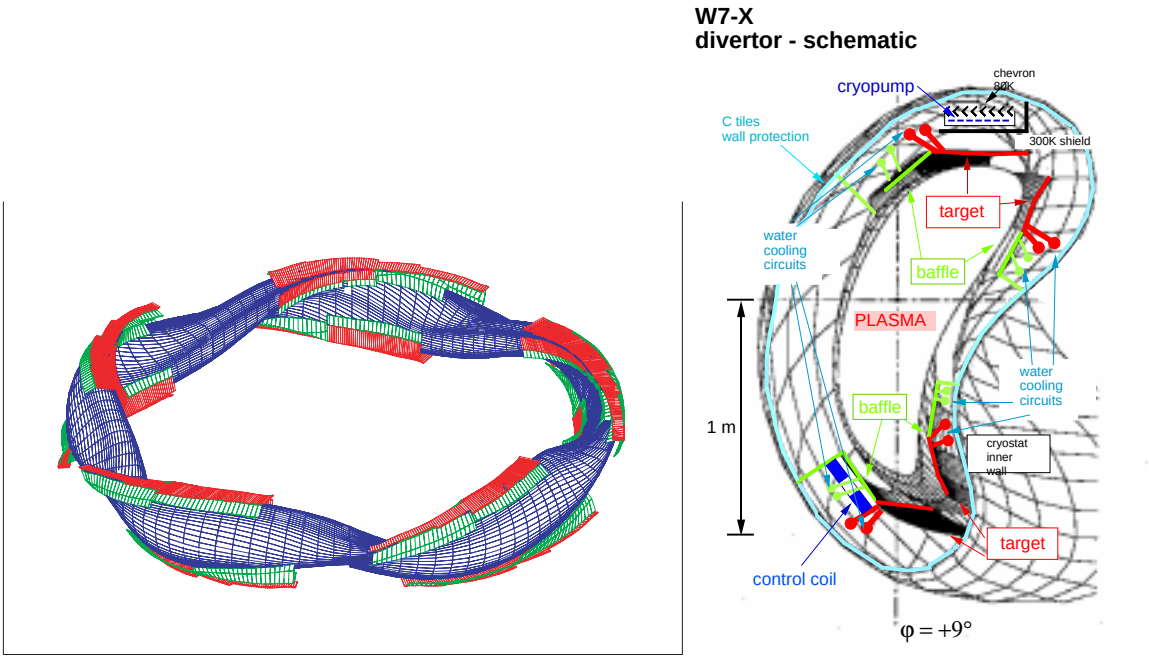

Figure 2.
Left: Target (red) and baffle plates (green) for the W7-X island divertor.
Right: Plasma cross section with details of the W7-X island divertor design.

However, this zone is limited to a rather small radial extent and a first estimate of the corresponding heat diffusion coefficient gives for this region a rather low value of about $5\,m^2/s$. Therefore, W7-X seems not to operate in regimes with dominating ergodic effects. Still, a more complete analysis of their influences has to be done with tools also necessary for other ergodic configurations like the dynamic ergodic divertor of TEXTOR [15].

Concerning high confinement modes, one can do shape variations in W7-X to avoid the X-point in bad curvature regions.

5. Specific aspects of the island divertor

The island divertor has specific physics aspects different from the axisymmetric divertor [16]. First of all, it has a different topology, because it has a region of closed fieldlines (the island) close to the core. This topology effect was studied with 2-D (toroidally averaged) calculations and it was found that in addition to the neutral losses through streaming of the plasma towards the target plates in this closed-fieldline region of the island (convective) momentum losses (driven through the large gradients) even at plasma temperatures well above 10 eV [17].

The dominting feature of these plasma configurations is particle accumulation inside the island [18, 19] by trapping the recycled neutrals (see Fig. 3). As a consequence a current flow pattern (see Fig. 3) is created which establishes a potential profile favouring this density distribution by adopting a maximum near the separatrix and in general being very different fron the simple $\Phi = 3kT$ ansatz. The island divertor is much more sensitive to effects of drifts, because the pitch is a factor of 10 to 50 smaller than in tokamaks amplifying by this these effects [20, 19].

Full 3D codes [21] indicate an additional momentum loss process through poloidal diffusion into shadowed regions and onset of trapped flow in this region. Counteracting of this

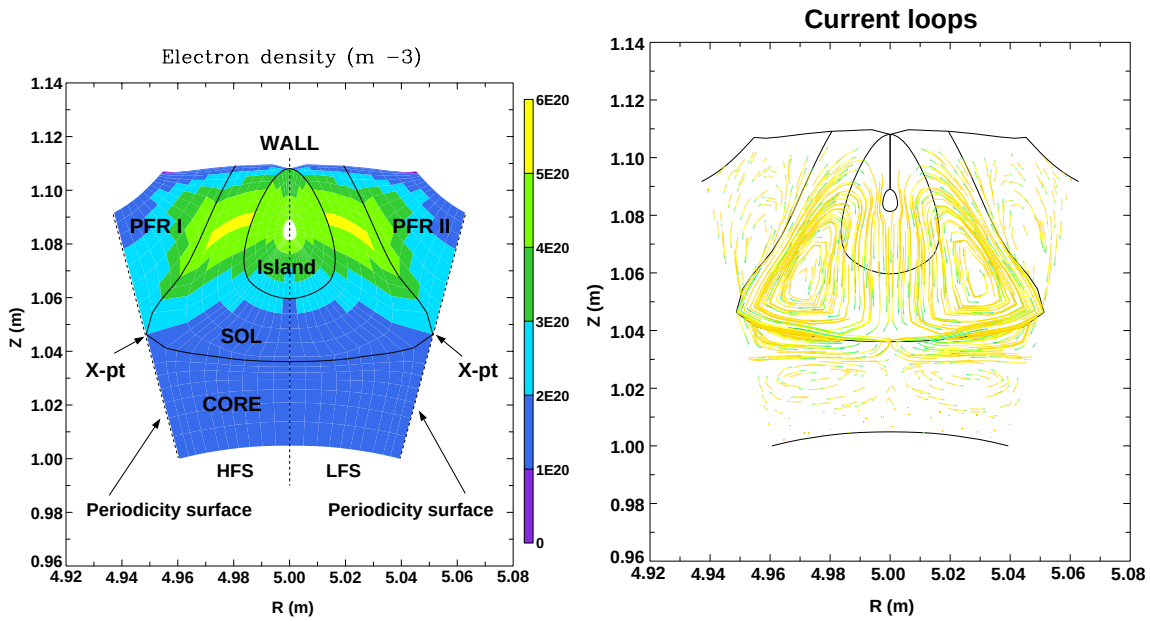

Figure 3.
Left: Typical density distribution obtained for a no-drifts high-recycling case. The island, core, SOL and private flux regions (PFR I and II), their boundaries, X-points and periodicity surfaces are also shown. HFS: High-field side; LFS: Low-field side.

Right: Test charge trajectories illustrating the current flow loops present in the plasma.

trapped flow with the main flow causes additional momentum loss by poloidal diffusion and shear viscosity. This leads to a deviation from the simple 2-point scaling [22]. Experimental results from W7-AS with island divertor operation [22] show also no onset of high recycling but a direct transfer to detached operation in agreement with 3D simulations. However, one can speculate that this might change for cleaner plasma conditions (as expected for a larger machine as W7-X). Lower impurity levels will avoid this tunneling through high-recycling conditions, because it avoids this upstream-driven detachment through impurities before enough recycling is established in the divertor.

The detachment dynamics is similar to standard tokamaks with a movement of the detachment front from the target to the X-point [22]. Possible instabilities occur then only when the radiation zone extends into the core region. From analysis of impurity-dominated regimes in tokamaks the formation of instablities (MARFEs) in the core region is well known. Simulations also show that these condensation instabilities have the tendency to redirect a part of the power-flow around it [23]. Therefore, the existence of local radiation instabilities in 3D stellarators can affect the power distribution on the different target plates. The same is true for the drifts. Therefore, the question of active vs. deactive islands and the need for control systems to symmetrize the different islands might get quite important.

Due to the small distance of the target plates from the core a later optimisation of the divertor might involve neutral baffle structures inside the island to shield the core by lowering the core influx of neutrals from the islands. Given the possibility of additional recycling at places not expected (like the main chamber recycling in tokamaks) this might be not too important. Nevertheless, the relative importance of wall recycling vs. divertor recycling has

to be evaluated.

Experimentally, by changing the pitch in the island, one has a nice tool to fine-tune the setup such that one can influence actively the competition between parallel (classical) and radial (anomalous) transport for relaxing the power load at the target plates.

One common problem for all decices is the need for a correct mapping algorithm allowing the comparison of different experiments (and including as one part the knowledge of the separatrix position). For a 3D device this might be a further challenge.

6. Summary

The island divertor of W7-X is based on design criteria as known from tokamaks. It is an open divertor not limiting the experimental scenarios and allowing a flexible start-up of the machine. In addition to common features as known from tokamaks, the 3D effects are of special interest. They might offer additional flexibility but might also cause additional problems to be counter-acted e.g. by feedback control.

Experimental results from W7-AS with an island divertor support the basic concept of the W7-X design.

7. References

[1] G. Grieger, W. Lotz, P. Merkel, J. Nührenberg, J. Sapper, et al., Physics optimization of stellarators, Phys. of Fluids B4 (1992), 2081–2091.

[2] WVII-A team, NI group, Plasma Physics and Controlled Nucl. Fusion Research, Vol. 1, IAEA Vienna (1981), 185.

[3] ITER physics base editors, ITER physics expert groups, JCT, Nucl. Fusion 39 (1999) 2137.

[4] H.-S. Bosch, D. Coster, S. Deschka, W. Engelhardt, C. García-Rosales, et al., Technical Report 1/281a, IPP, Garching, Germany, 1994.

[5] M. Keilhacker, K. Lackner, K. Behringer, H. Murmann, and H. Niedermeyer, Physica Scripta T2/2 (1982) 443.

[6] K. Borrass and P. Stangeby, in *Europhysics Conference Abstracts (Proc. of the 20th EPS Conference on Controlled Fusion and Plasma Physics, Lisbon, 1993)*, edited by J. A. Costa Cabral, M. E. Manso, F. M. Serra, and F. C. Schüller, volume 17C, part II, pages 763–766, Petit-Lancy, 1993, EPS.

[7] K. Borrass and G. Janeschitz, Nucl. Fusion 34 (1994) 1203.

[8] C. S. Pitcher, H.-S. Bosch, A. Carlson, J. C. Fuchs, G. Haas, et al., in *Europhysics Conference Abstracts (Proc. of the 22th EPS Conference on Controlled Fusion and Plasma Physics, Bournemouth, 1995)*, edited by B. Keen, P. Stott, and J. Winter, volume 19C, part III, pages 245–248, Geneva, 1995, EPS.

[9] K. Borrass, R. Schneider, and R. Farengo, Nucl. Fusion 37 (1997) 523.

[10] R. Schneider, H.-S. Bosch, D. Coster, J. Fuchs, J. Gafert, et al., J. Nucl. Mater. 266–269 (1999) 175.

[11] A. Herrmann, J. C. Fuchs, V. Rohde, M. Weinlich, and ASDEX Upgrade Team, J. Nucl. Mater. 266–269 (1999) 291.

[12] A. Kallenbach, M. Kaufmann, D. P. Coster, J. C. Fuchs, A. Herrmann, et al., Nucl. Fusion 39 (1999) 901.

[13] H. Renner, J. Boscary, V. Erckmann, H. Greuner, H. Grote, et al., Nucl. Fusion 40 (2000) 1083.

[14] E. Strumberger, J. Nucl. Mater. 266–269 (1999) 1207.

[15] K. Finken, T. Eich, S. Abdullaev, A. Klaeck, G. Mank, et al., J. Nucl. Mater. 266–269 (1999) 495.

[16] F. Sardei, Y. Feng, J. Kisslinger, and W7-AS team, Contrib. Plasma Physics 40 (2000) 238, 7th International Workshop on Plasma Edge Theory, October 1999, Tajimi, Japan.
[17] G. Herre, , P. Grigull, and R. Schneider, J. Nucl. Mater. 266–269 (1999) 1015.
[18] F. Sardei, Y. Feng, P. Grigull, G. Herre, D. Hildebrandt, et al., J. Nucl. Mater. 241–243 (1997) 135.
[19] X. Bonnin, R. Schneider, D. Coster, V. Rozhansky, and S. Voskoboynikov, J. Nucl. Mater. 290–293 (2001) 829.
[20] Y. Feng, F. Sardei, and J. Kisslinger, J. Nucl. Mater. 266–269 (1999) 812.
[21] Y. Feng, G. Herre, P. Grigull, et al., Plasma Phys. Controlled Fusion 40 (1998) 371.
[22] R. Koenig, this conference.
[23] H. Kastelewicz et al., Plasma Phys. Controlled Fusion 37 (1995) 723.